

Pressure-induced band gap closing of lead-free halide double perovskite $(CH_3NH_3)_2PtI_6$

Siyu Hou(侯思羽), Jiaxiang Wang(王家祥), Yijia Huang(黄乙甲), Ruijing Fu(付瑞净), and Lingrui Wang(王玲瑞)
Citation: Chin. Phys. B, 2025, 34 (**8**): 086106. DOI: 10.1088/1674-1056/adce9e
http://cpb.iphy.ac.cn; http://iopscience.iop.org/cpb

What follows is a list of articles you may be interested in

Synergistic improvements in mechanical and thermal performance of TiB_2 solid-solution-based composites

Zhuang Li(李壮), Cun You(由存), Zhihui Li(李志慧), Xuepeng Li(李雪鹏), Guiqian Sun(孙贵乾), Xinglin Wang(王星淋), Qi Jia(贾琪), Qiang Tao(陶强), and Pinwen Zhu(朱品文)
Chin. Phys. B, 2025, 34 (**8**): 086105. DOI: 10.1088/1674-1056/add00c

Morphology-tuned phase transition of MnO_2 nanorods under high pressure

Xue-Ting Zhang(张雪婷), Chen-Yi Li(李晨一), Hui Tian(田辉), Xin-Yue Wang(王心悦), Zong-Lun Li(李宗伦), and Quan-Jun Li(李全军)
Chin. Phys. B, 2025, 34 (**6**): 066105. DOI: 10.1088/1674-1056/adc192

Layer-dependent structural stability and electronic properties of $CrPS_4$ under high pressure

Jian Zhu(朱健), Dengman Feng(冯登满), Liangyu Wang(王亮予), Liang Li(李亮), Fangfei Li(李芳菲), Qiang Zhou(周强), and Yalan Yan(闫雅兰)
Chin. Phys. B, 2025, 34 (**6**): 066102. DOI: 10.1088/1674-1056/adc65f

Well defined phase boundaries and superconductivity with high T_c in PbSe single crystal

Jiawei Hu(胡佳玮), Yanghao Meng(孟养浩), He Zhang(张赫), Wei Zhong(钟韦), Hang Zhai(翟航), Xiaohui Yu(于晓辉), Binbin Yue(岳彬彬), and Fang Hong(洪芳)
Chin. Phys. B, 2025, 34 (**4**): 046102. DOI: 10.1088/1674-1056/adb272

First-principles insights into the high-pressure stability and electronic characteristics of molybdenum nitride

Tao Wang(王涛), Ming-Hong Wen(温铭洪), Xin-Xin Zhang(张新欣), Wei-Hua Wang(王伟华), Jia-Mei Liu(刘佳美), Xu-Ying Wang(王旭颖), and Pei-Fang Li(李培芳)
Chin. Phys. B, 2025, 34 (**3**): 036104. DOI: 10.1088/1674-1056/adab66

SPECIAL TOPIC — Structures and properties of materials under high pressure

Pressure-induced band gap closing of lead-free halide double perovskite $(CH_3NH_3)_2PtI_6$

Siyu Hou(侯思羽)[1], Jiaxiang Wang(王家祥)[1], Yijia Huang(黄乙甲)[1], Ruijing Fu(付瑞净)[2,†], and Lingrui Wang(王玲瑞)[1,‡]

[1] *Key Laboratory of Materials Physics, Ministry of Education, School of Physics, Zhengzhou University, Zhengzhou* 450001, *China*
[2] *School of Applied Physics and Materials, Wuyi University, Jiangmen* 529020, *China*

(Received 27 February 2025; revised manuscript received 17 April 2025; accepted manuscript online 21 April 2025)

Lead-free halide double perovskites have recently attracted significant attention due to their exceptional stability and favorable band gaps, making them promising candidates for solar cell applications. However, the relationship between their structural characteristics and intrinsic band gap remains under-explored. This study presents a method to investigate the structure-band gap correlation in a typical halide double perovskite, MA_2PtI_6 ($MA^+ = CH_3NH_3^+$), using high pressure techniques. The band gap of MA_2PtI_6 is effectively reduced at two different rates of 0.063 eV/GPa and 0.079 eV/GPa before and after 1.2 GPa, and progressively closes as pressure further increases. These optical changes are closely related to the pressure induced structural evolution of MA_2PtI_6. Moreover, a phase transition from trigonal (R-3m) to monoclinic ($P2/m$) occurs at 1.2 GPa and completes by 2.0 GPa, driven by pressure-induced distortion of the $[PtI_6]^{2-}$ octahedra, which is responsible for the variation of the band gap. These promising findings pave the way for potential applications in the structural and band gap tuning of halide double perovskites.

Keywords: halide double perovskites, high pressure, band gap closing, phase transition

PACS: 61.50.Ks, 62.50.–p, 78.40.Fy

DOI: 10.1088/1674-1056/adce9e **CSTR:** 32038.14.CPB.adce9e

1. Introduction

Lead-free halide double perovskites (A_2BX_6, X = Cl, Br, and I), in contrast to lead-based halide perovskites ($APbX_3$), are distinguished by their enhanced stability under diverse environmental conditions, eco-friendliness due to the absence of harmful Pb, and ease of processing, positioning them as promising green photovoltaic materials.[1–3] On one hand, the structure of A_2BX_6 features shorter and stronger B–X bonds compared to the Pb–X bonds in $APbX_3$, resulting in improved stability against water and oxygen.[4,5] On the other hand, the shorter and stronger B–X bonds also significantly influence the electronic structure of halide double perovskites A_2BX_6, leading to increased electron cloud overlap, a smaller band gap, and a more favorable alignment with the solar spectrum for high power conversion efficiency.[6,7] Despite these advantages, understanding their fundamental structure–optical properties remains essential for practical applications.

High pressure is an effective technique for precisely tuning optical properties by shortening atomic distances and enhancing electron orbital coupling, thereby altering the electronic and crystal structures and providing deeper insights into the structure–optical properties relationship.[8–11] Recent studies have demonstrated that applying high pressure to perovskites can induce various changes, including shape changes, phase transitions, band gap modulation, and alterations in carrier dynamics.[12–15] For instance, Li *et al.*[16,17] employed high pressure to tune the band gap of lead-free $Cs_2AgBiBr_6$ double perovskite, offering new perspectives for the development of advanced perovskite-based devices. Wang *et al.*[18] and Meng *et al.*[19] observed dramatic piezoceramics in $(NH_4)_2SeBr_6$, along with the formation of Br–Br bonds between the $[SeBr_6]^{2-}$ octahedra, marking the first observation of such a phenomenon in halide perovskites. Therefore, it is essential to investigate the structure–optical properties of double halide perovskites through pressure engineering.

Here, we systematically investigate the pressure-dependent structure–optical properties of the double perovskite MA_2PtI_6 ($MA^+ = CH_3NH_3^+$) using *in situ* high pressure ultraviolet-visible (UV-vis) absorption, angle-dispersive x-ray diffraction (ADXRD), Raman, and infrared (IR) spectroscopy. The results reveal that MA_2PtI_6 undergoes a structural phase transition from trigonal (R-3m) to monoclinic ($P2/m$). As the pressure increases, the absorption edge of MA_2PtI_6 exhibits a gradual red shift, while its intrinsic band gap continuously narrows. This study deepens the understanding of the structure–optical properties of lead-free halide double perovskites and paves the way for future advancements in their optoelectronic applications.

†Corresponding author. E-mail: ruijingfu_wyu@163.com
‡Corresponding author. E-mail: wanglr@zzu.edu.cn

© 2025 Chinese Physical Society and IOP Publishing Ltd. All rights, including for text and data mining, AI training, and similar technologies, are reserved.

2. Experimental methods

2.1. Sample preparation and high pressure generation

The crystal of MA_2PtI_6 was synthesized according to the procedure described in previous reports.[20] The simulated ambient structure of MA_2PtI_6 was generated using CCDC-1848509.[20]

In situ high pressure experiments were conducted using a symmetric DAC apparatus equipped with a pair of 400 μm culet diamonds at ambient conditions. A T301 stainless steel gasket was pre-indented by the diamonds and drilled to create a 150 μm diameter cavity for sample loading. The crystal sample was enclosed within the gasket hole along with a ruby ball for pressure determination via the standard ruby fluorescence technique. Mineral oil was employed as the pressure-transmitting medium.

2.2. High pressure experiment

In situ high-pressure optical and structural characterizations, including absorption, Raman, IR, and ADXRD measurements, were carried out using the following setups:

Absorption measurements were performed using a deuterium–halogen light source (DH-2000-BAL, Ocean Insight) and an optical fiber spectrometer (QE65PRO, Ocean Insight), with additional components provided by Light & Microvision Industrial Technology Co., Ltd.

Raman measurements were conducted using a 532 nm, 8 mW excitation laser (MSL-U-532 nm, Cnilaser) and a Raman spectrometer (HRS-500MS, Princeton Instruments) coupled to a high-sensitivity, thermoelectrically cooled charge-coupled device (CCD) detector (PIX-256E, Princeton Instruments).

IR measurements were conducted using a Nicolet iN10 FT-IR micro-spectrometer.

ADXRD experiments were conducted at the 15U1 beamline, Shanghai Synchrotron Radiation Facility (SSRF).

3. Results and discussion

Considering the important role of the band gap in photovoltaic field, we conducted *in situ* high-pressure UV-vis absorption spectroscopy experiments to show the pressure effect on optical properties of MA_2PtI_6.[20,21] The absorption spectra of MA_2PtI_6 under high pressure are shown in Fig. 1(a). It can be observed that the absorption edge of MA_2PtI_6 exhibits a continuous red shift as pressure increases, progressively moving into the infrared and fully transitioning into the infrared region at 10.2 GPa. The absorption spectrum almost returns to its initial state upon decompression, as illustrated in Fig. 1(b). Furthermore, we used the Tauc plot method to calculate the band gap values of MA_2PtI_6 at different pressures. Previous works have indicated that MA_2PtI_6 shows the nature of an indirect band gap.[22,23] As shown in Fig. 1(c), the band gap of MA_2PtI_6 at ambient conditions is 1.32 eV. We obtained the band gaps of MA_2PtI_6 at various pressures, as depicted in Fig. 1(d), and conducted a linear fit on these values. The rate of band gap reduction before 1.2 GPa is 0.063 eV/GPa, while beyond this pressure, it increases to 0.079 eV/GPa. This phenomenon indicates that MA_2PtI_6 may undergo a structural phase transition at 1.2 GPa. It is well known that the $[PtI_6]^{2-}$ octahedra are responsible for the alterations in the electronic structure near the band edges, thereby determining the band gap.[24] The observed decrease in the band gap of MA_2PtI_6 reflects alterations in the electronic structure, driven by the evolving configuration of the $[PtI_6]^{2-}$ octahedra.

To further identify the microscopic mechanism of structural changes and their correlation with the optical properties of MA_2PtI_6, we carried out *in situ* high pressure ADXRD experiments. The maximum pressure achieved in our experiment was 21.3 GPa (Fig. 2(a)). The initial ADXRD pattern at 0.0 GPa reveals that the MA_2PtI_6 structure is the pure trigonal phase with the space group *R*-3*m*, consistent with previous studies.[20] As pressure increases, all diffraction peaks shift to higher angles, indicating the pressure-induced decrease in lattice parameters. However, new peaks emerge at 1.2 GPa, signaling the occurrence of a phase transition.[25,26] By 2.0 GPa, the phase transition is complete, indicating the presence of a phase transition zone between 1.2 GPa and 2.0 GPa. This new phase persists up to 21.3 GPa. In Fig. 2(b), the refinement of the simulated ADXRD patterns corresponds well with the experimental data. At ambient conditions, the ADXRD pattern matches the trigonal phase, and the Pawley refinement yields lattice parameters of $a = b = 7.9597(2)$ Å, $c = 22.79(1)$ Å, $\alpha = \beta = 90°$ and $\gamma = 120°$. At 2.5 GPa, Pawley refinement shows that it matches the monoclinic phase (*P*2/*m*) with lattice parameters of $a = 7.7165(3)$ Å, $b = 8.1418(9)$ Å, $c = 23.9169(1)$ Å, $\alpha = 90°$, $\beta = 91.95(1)°$, and $\gamma = 90°$.[27] The refinement R factors are $R_p = 2.00\%$ and $R_{wp} = 0.99\%$ at 2.5 GPa, confirming that MA_2PtI_6 undergoes a phase transition with symmetry reduction from trigonal to monoclinic phase under high pressure.[28] From the above discussion, a phase transition zone between 1.2 GPa and 2.0 GPa is evident, during which the structure transforms from trigonal (*R*-3*m*) to monoclinic (*P*2/*m*). This transition is driven by the progressive distortion of the $[PtI_6]^{2-}$ octahedra, particularly the changes in Pt–I bond lengths and I–Pt–I bond angles, which result in variations in the slope of band gap reduction. Moreover, this new monoclinic phase remains stable up to 21.3 GPa. Upon decompression, the crystal structure of MA_2PtI_6 reverts to its original trigonal phase (space group *R*-3*m*). Pawley refinement of the released ADXRD pattern yields lattice parameters of $a = b = 7.9139(1)$ Å, $c = 22.4742(1)$ Å, $\alpha = \beta = 90°$ and $\gamma = 120°$. This reversibility indicates that the pressure-induced monoclinic phase transition is reversible, exhibiting some degree of pressure hysteresis, with the material returning to its

original structural state upon pressure release.[29]

The variations in cell volume and cell parameters of MA_2PtI_6 upon compression are presented in Fig. 3. To account for the pressure-induced stiffening of the MA_2PtI_6 lattice, we fit their pressure–volume relationships to the third order Birch–Murnaghan equation of state (Fig. 3(a)) as[30,31]

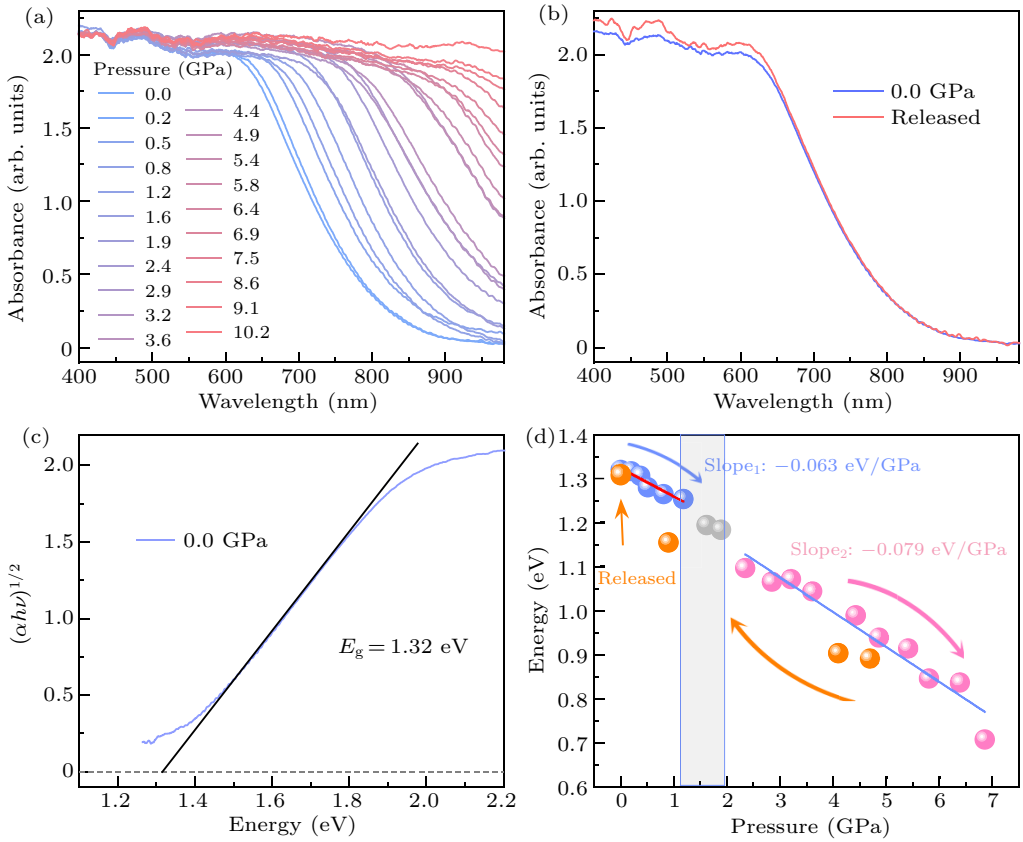


Fig. 1. (a) Selected optical absorption spectra of MA_2PtI_6 under varying pressure. (b) Comparison of the optical absorption spectra of MA_2PtI_6 at ambient conditions and after pressure release. (c)–(d) The indirect band gap Tauc plot under ambient conditions and the band gap evolution of MA_2PtI_6 during compression and decompression, respectively. The symbol size covers the size of the error bars. The shaded area represents the phase transition zone.

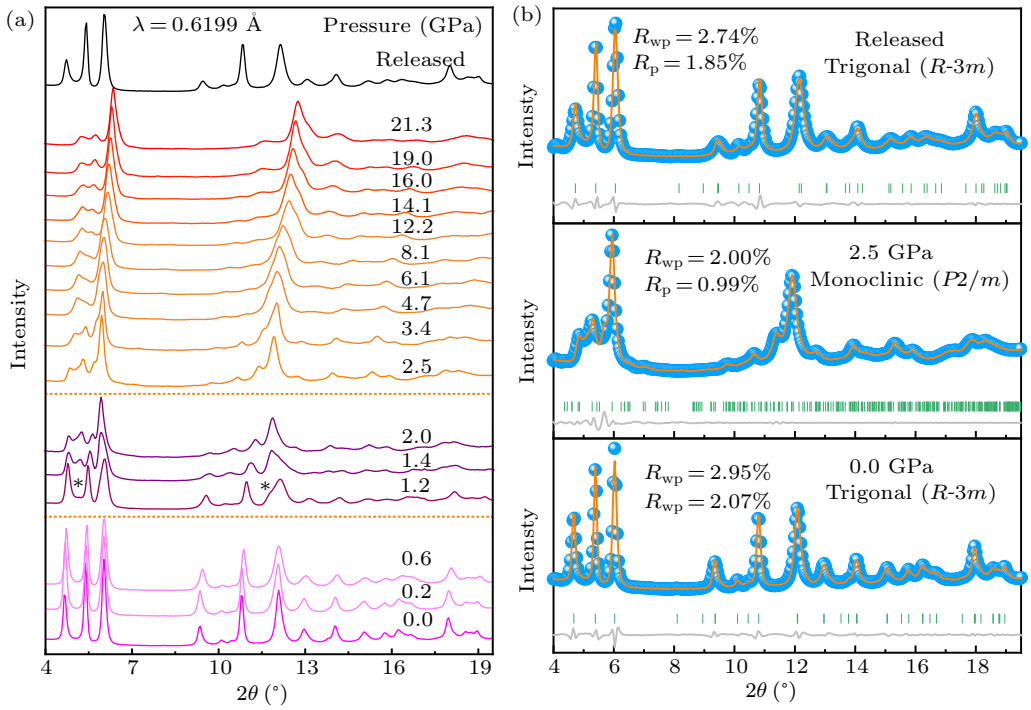


Fig. 2. (a) Pressure-dependent *in situ* synchrotron ADXRD patterns of MA_2PtI_6 in compression up to 21.3 GPa. The phase transition is concluded since new peaks can be identified. (b) Refinements of the experimental ADXRD data at 0.0 GPa, 2.5 GPa and after decompression to ambient conditions.

$$P(V) = \frac{3B_0}{2}\left[\left(\frac{V_0}{V}\right)^{7/3} - \left(\frac{V_0}{V}\right)^{5/3}\right] \times \left\{1 + \frac{3}{4}(B_0' - 4)\left[\left(\frac{V_0}{V}\right)^{2/3} - 1\right]\right\},$$

where B_0 is the bulk modulus at atmospheric pressure, B_0' is a parameter for the pressure derivative, and V_0 is the zero pressure volume. Under pressure, MA_2PtI_6 exhibits significant changes in compressibility below 1.2 GPa. As pressure increases, the pressure–volume profile exhibits a discontinuous change. Fitting the third-order Birch–Murnaghan equation of state for the monoclinic phase of MA_2PtI_6 yields $B_0 = 42.49$ GPa, indicating low compressibility. To further study the structural variation, we investigate the evolution of lattice constants of MA_2PtI_6 upon compression. The high pressure behavior of the a axis is found to be equal to that of the b axis, while the compressibility of the a (b) and c axes is anisotropic under mild pressure (< 1.2 GPa) (Fig. 3(b)). Notably, the three axes (a, b, and c) show different compression rates beyond 1.2 GPa. This indicates that the local structure of the $[PtI_6]^{2-}$ octahedra has been distorted, which in turn alters the electronic cloud distribution within the $[PtI_6]^{2-}$ coordination, and is responsible for the band gap closing observed during compression.

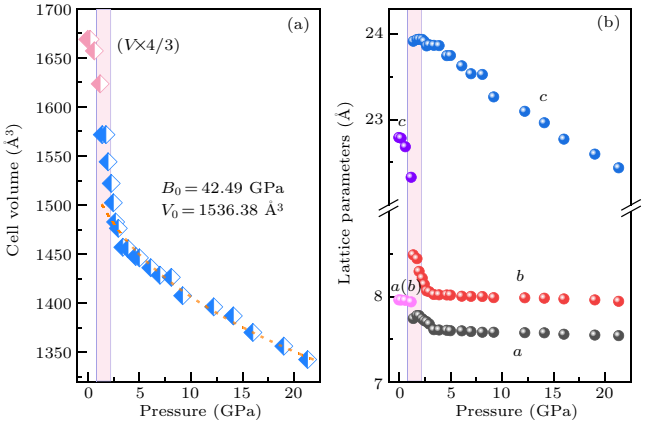


Fig. 3. (a) Pressure dependence of the unit cell volume of MA_2PtI_6 fitted by the third-order Birch–Murnaghan equation of state. (b) Lattice parameters at different pressure. The shaded area represents the phase transition zone. Initially, the unit cell contains $Z = 3$, and after the phase transition, it contains $Z = 4$. Therefore, "$V \times 4/3$" is utilized to more effectively compare the volume changes before and after the phase transition.

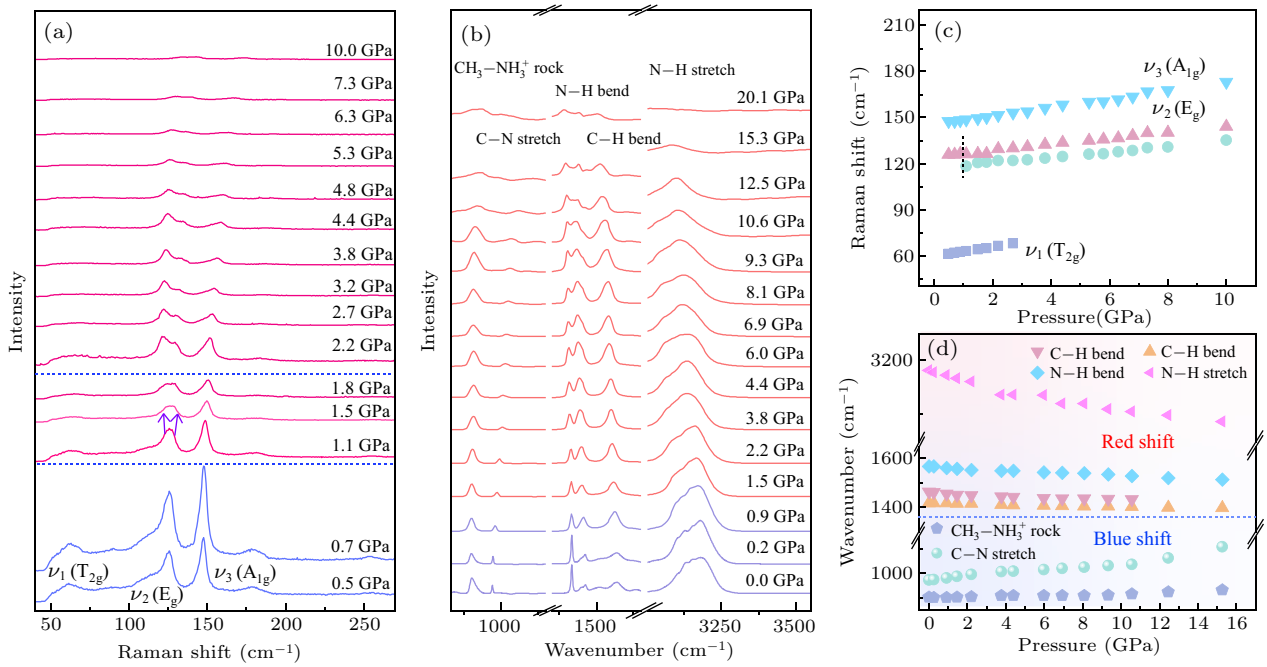


Fig. 4. (a) High pressure Raman spectra of MA_2PtI_6 in the region of 40–280 cm^{-1} and (c) the corresponding frequency shift with increasing pressure. (b) High pressure IR spectra of MA_2PtI_6 and (d) the corresponding frequency shift as pressure increases.

We also performed *in situ* high-pressure IR spectroscopy experiments to investigate the impact of structural changes in the inorganic octahedron on the local lattice vibrations of MA_2PtI_6 and the high pressure behavior of the organic MA^+ cations under compression. Figures 4(a) and 4(c) show the *in situ* Raman spectra of MA_2PtI_6 and the corresponding frequency shifts as a function of pressure. Under ambient conditions, three main Raman vibrational modes in the low wavenumber range of 40–280 cm^{-1} can be observed, corresponding to lattice vibrations associated with Pt–I vibration. Based on previous studies, the band at 61 cm^{-1} corresponds to the triply degenerate bending vibration ν_1 (T_{2g}), the band at 126 cm^{-1} corresponds to the antisymmetric stretching vibration ν_2 (E_g), and the band at 148 cm^{-1} corresponds to the symmetric stretching vibration ν_3 (A_{1g}).[32] As pressure increases, all modes shift to higher frequencies, consistent with the contraction of the $[PtI_6]^{2-}$ octahedron and the reduction of the band gap. It can be observed that the ν_2 peak broadens at 1.1 GPa and subsequently splits into two modes with increasing pressure, indicating local distortion in the $[PtI_6]^{2-}$

octahedron. The pressure-induced Raman peak variations of MA_2PtI_6 are consistent with its XRD evolution, reflecting the structural transition under compression. Given that hydrogen bonding connects the organic MA^+ part and the inorganic $[PtI_6]^{2-}$ octahedron, we further performed *in situ* IR spectroscopy to explore the vibrational modes of MA^+. As shown in Figs. 4(b) and 4(d), the vibrational modes related to the organic group $CH_3NH_3^+$ rock (901 cm^{-1}) and C–N (970 cm^{-1}) stretch exhibit a blue shift with increasing pressure, indicating significant hardening of the organic cations, enhanced C–N interactions and reduced bond lengths. In contrast, the stretching of N–H observed at 3000 and 3250 cm^{-1}, along with the bending of C–H and N–H modes in the IR spectra between 1400 and 1600 cm^{-1}, exhibits a substantial red shift, signifying the strengthening of hydrogen bonding between the organic MA^+ cations and the inorganic $[PtI_6]^{2-}$ octahedra.[33–36] The high pressure Raman and IR results reveal that the organic MA^+ skeleton undergoes minor distortion, while the $[PtI_6]^{2-}$ octahedra undergo significant tilting distortions, with both components remaining interconnected through hydrogen bonding. Hence, it can be concluded that the asymmetry of MA^+, mediated by hydrogen bonding interactions with the surrounding I ions, influences the $[PtI_6]^{2-}$ octahedra and subsequently alters the optical properties.

4. Conclusions

In summary, we successfully narrowed the band gap of MA_2PtI_6 through high-pressure treatment. Under high pressure, the band gap of MA_2PtI_6 decreases with two distinct rates, resulting from the shrinkage and distortion of $[PtI_6]^{2-}$ coordinated environment. These inorganic local structural changes, including shrinkage and distortion, induce a phase transition from trigonal (R-3m) to monoclinic ($P2/m$). Additionally, the MA^+ organic skeleton undergoes distortion through hydrogen bonding interactions. The hydrogen bond between the asymmetric organic cation and the inorganic framework strengthens under high pressure, affecting the inorganic $[PtI_6]^{2-}$ octahedra and, consequently, the optical properties. This work demonstrates the critical role of high pressure in modifying both the band gap and structure, offering deeper insights into the structure–property relationships of halide double perovskites for their future photovoltaic applications.

Acknowledgements

This work was supported by the National Natural Science Foundation of China (Grant No. 12474414), the Natural Science Foundation of Henan (Grant No. 242300421157), and the ADXRD measurement was performed at the 4W2 beamline, the Beijing Synchrotron Radiation Facility (BSRF).

References

[1] Igbari F, Wang Z K and Liao L S 2019 *Adv. Energy Mater.* **9** 1803150
[2] Zhao X G, Yang D, Ren J C, Sun Y, Xiao Z and Zhang L 2018 *Joule* **2** 1662
[3] Wolf N R, Connor B A, Slavney A H and Karunadasa H I 2021 *Angew. Chem. Int. Ed.* **60** 16264
[4] Lee B, Stoumpos C C, Zhou N, Hao F, Malliakas C, Yeh C Y, Marks T J, Kanatzidis M G and Chang R P H 2014 *J. Am. Chem. Soc.* **136** 15379
[5] Chu Y, Hu Y and Xiao Z 2021 *J. Phys. Chem. C* **125** 9688
[6] Zhao X G, Yang J H, Fu Y, Yang D, Xu Q, Yu L, Wei S H and Zhang L 2017 *J. Am. Chem. Soc.* **139** 2630
[7] Qiu X, Cao B, Yuan S, Chen X, Qiu Z, Jiang Y, Ye Q, Wang H, Zeng H, Liu J and Kanatzidis M G 2017 *Sol. Energy Mater. Sol. Cells* **159** 227
[8] Kong L, Liu G, Gong J, Mao L, Chen M, Hu Q, Lü X, Yang W, Kanatzidis M G and Mao H K 2020 *Proc. Natl. Acad. Sci. USA* **117** 16121
[9] Ma Z, Liu Z, Lu S, Wang L, Feng X, Yang D, Wang K, Xiao G, Zhang L, Redfern S A T and Zou B 2018 *Nat. Commun.* **9** 4506
[10] Guo S, Mihalyi-Koch W, Mao Y, Li X, Bu K, Hong H, Hautzinger M P, Luo H, Wang D, Gu J, Zhang Y, Zhang D, Hu Q, Ding Y, Yang W, Fu Y, Jin S and Lü X 2024 *Nat. Commun.* **15** 3001
[11] Lü X, Wang Y, Stoumpos C C, Hu Q, Guo X, Chen H, Yang L, Smith J S, Yang W, Zhao Y, Xu H, Kanatzidis M G and Jia Q 2016 *Adv. Mater.* **28** 8663
[12] Wang J, Wang L, Li Y, Fu R, Feng Y, Chang D, Yuan Y, Gao H, Jiang S, Wang F, Guo E, Cheng J, Wang K, Guo H and Zou B 2022 *Adv. Sci.* **9** 2203442
[13] Wang J, Yuan Y, Liu C, Fu R, Wang L, Zhang F, Ma L, Jiang S, Shi Z and Guo H 2023 *Phys. Rev. B* **107** 214111
[14] Zhao D, Xiao G, Liu Z, Sui L, Yuan K, Ma Z and Zou B 2021 *Adv. Mater.* **33** 2100323
[15] Sun X, Wu M, Yu X, Li Q, Xiao G, Wang K and Zou B 2024 *Adv. Sci.* **11** 2306937
[16] Li Q, Wang Y, Pan W, Yang W, Zou B, Tang J and Quan Z 2017 *Angew. Chem. Int. Ed.* **56** 15969
[17] Li Q, Li S, Wang K, Quan Z, Meng Y and Zou B 2017 *J. Phys. Chem. Lett.* **8** 500
[18] Wang L, Yao P, Wang F, Li S, Chen Y, Xia T, Guo E, Wang K, Zou B and Guo H 2020 *Adv. Sci.* **7** 1902900
[19] Meng L, Vu T V, Criscenti L J, Ho T A, Qin Y and Fan H 2023 *Chem. Rev.* **123** 10206
[20] Evans H A, Fabini D H, Andrews J L, Koerner M, Preefer M B, Wu G, Wudl F, Cheetham A K and Seshadri R 2018 *Inorg. Chem.* **57** 10375
[21] Fu R, Chen Y, Yong X, Ma Z, Wang L, Lv P, Lu S, Xiao G and Zou B 2019 *Nanoscale* **11** 17004
[22] Tauc J, Grigorovici R and Vancu A 1966 *Phys. Stat. Sol. (b)* **15** 627
[23] Liu D, Zhang C and Sa R 2022 *Phys. B: Condens. Matter* **644** 414235
[24] Bu K, Feng X, Wang D, *et al.* 2024 *J. Am. Chem. Soc.* **146** 22469
[25] Li Q, Xu B, Chen Z, Han J, Tan L, Luo Z, Shen P and Quan Z 2021 *Adv. Funct. Mater.* **31** 2104923
[26] Cao Y, Qi G, Sui L, *et al.* 2020 *ACS Mater. Lett.* **2** 381
[27] Togo A and Tanaka I 2013 *Phys. Rev. B* **87** 184104
[28] Feng C, Zhao Q, Wu C, Luo X, Li S, Li D, Tang G, Zhang G 2022 *J. Phys. Chem. Lett.* **13** 1077
[29] Szafrański M 2024 *J. Mater. Chem. A* **12** 2391
[30] Cliffe M J and Goodwin A L 2012 *J. Appl. Crystallogr.* **45** 1321
[31] Katsura T and Tange Y 2019 *Minerals* **9** 745
[32] Hamaguchi H O 1978 *J. Chem. Phys.* **69** 569
[33] Tian C, Liang Y, Chen W, Huang Y, Huang X, Tian F and Yang X 2020 *Phys. Chem. Chem. Phys.* **22** 1841
[34] Wang J, Wang L, Wang F, Jiang S and Guo H 2021 *Phys. Chem. Chem. Phys.* **23** 19308
[35] Wang L, Wang K, Xiao G, Zeng Q and Zou B 2016 *J. Phys. Chem. Lett.* **7** 5273
[36] Mao Y, Guo S, Huang X, *et al.* 2023 *J. Am. Chem. Soc.* **145** 23842